

**A STUDY ON PARAMETRIC ROLL MOTIONS
BY FULLY NONLINEAR NUMERICAL WAVE TANK**

Katsuji Tanizawa[†] and *Shigeru Naito*[‡]

[†] Ship Research Institute, Tokyo, Japan

[‡] Osaka University, Osaka, Japan

ABSTRACT

Parametric roll motion of a two-dimensional floating body is studied numerically, theoretically and experimentally. For numerical study, a fully nonlinear numerical wave tank is applied. This is a time domain simulation program which solves simultaneous equations of ideal fluid motion and floating body motions. To satisfy the radiation condition at the tank ends, an artificial damping technique is applied. Using this numerical wave tank, motions of a floating body in regular waves are simulated and the critical wave height, which excite the parametric roll oscillation, is estimated. Theoretical estimation of this criteria is also given from the stability analysis of coupled Mathieu type equation of heave and roll motions. To validate these numerical and theoretical results, an experiment is performed. Comparison among numerical, theoretical and experimental results show that the simulated motions well agree with the measured motions in both harmonic and parametric oscillations, and as a result, the criteria estimated by the numerical simulations agrees with the measured criteria qualitatively and quantitatively, meanwhile the theoretical criteria agrees qualitatively.

KEY WORDS : Parametric oscillation, Numerical wave tank, Fluid-body interaction, Fully nonlinear simulation, Acceleration potential, Implicit body surface boundary condition

INTRODUCTION

Responses of floating bodies such as ships or ocean structures to incident waves are one of the main concern in ocean engineering. The responses are usually treated as harmonic assuming small amplitude wave and body motions. Under the assumption, the frequency responses have been investigated by linear or perturbation theories. But, the body motions are not always harmonic in real ocean. When amplitude of wave and body motions are large in rough seas, nonlinear effects become dominant. Capsizing in the plunging breaker is the extreme example. Even if the amplitudes are small, nonlinearity due to body shape, mooring force, free water on the deck etc. affect to the body motions and chaotic or parametric motions may be resulted. In this paper, harmonic and parametric roll motions of a two-dimensional body are studied numerically, theoretically and experimentally.

Parametric roll motions are arising from the time dependent variation of the metacenter height of the body due to relative heave motions

to the free-surface. If the body has sensitive shape to parametric excitation, the roll angle diverges exponentially and results in capsizing. In particular, when the wave period is nearly equal to the half of the natural roll period, parametric motion is very easy to be excited even in a small amplitude wave.

For the analysis of parametric roll motions, time domain fully nonlinear simulation can be a powerful tool. Time domain fully nonlinear simulation methods are studied by Vinje⁵⁾, Cointe⁷⁾, Tanizawa^{8, 14)}, Kang⁹⁾, Van Daalen¹⁰⁾, Sen¹¹⁾, Cao¹²⁾ and others in the past decade and fully nonlinear numerical wave tanks have been developed. In this study, using the numerical wave tank¹⁵⁾, the parametric motion together with the harmonic motion are simulated seamlessly in time domain and the critical wave height, which excite the parametric motion, is estimated. For the validation of the numerical results, an experiment is performed.

The parametric oscillation is a classical problem and has been studied using Mathieu type model equations in a number of fields of science. So, also in this paper, Mathieu type simultaneous equations of heave and roll motions are composed and the criteria is estimated from the stability analysis of this model equations.

Through these studies, the applicability of the numerical wave basin to the parametric motions are discussed.

FULLY NONLINEAR NUMERICAL WAVE TANK

Mathematical formulation

Motions of a floating body inside a two-dimensional wave basin is considered. As Fig.1 shows, fluid domain Ω is bounded by free-surfaces S_f , a piston wave maker S_p , bottom and rigid wall S_b and a floating body S_s . Here, gravitational acceleration g , density of fluid ρ and width of floating body B are chosen as units to nondimensionalize the problem. An space-fixed Cartesian coordinate system $o-xz$ is used with x coincident with the calm free-surface and z positive upward. The fluid is assumed to be homogeneous, incompressible, inviscid and its motion irrotational. The fluid motion can be described by a velocity potential ϕ and its time derivative ϕ_t . In the fluid domain Ω , ϕ and ϕ_t satisfies Laplace's equation

$$\nabla^2 \phi = \nabla^2 \phi_t = 0 . \quad (1)$$

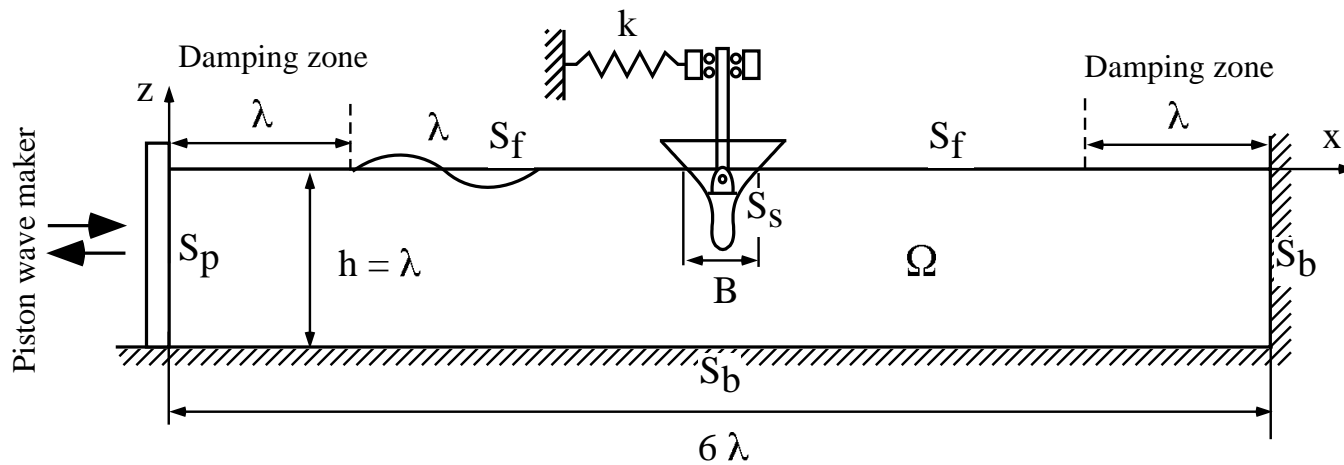


Fig.1 Simulation with damping zones

Green's second identity can be applied on both ϕ and ϕ_t

$$c(\mathcal{Q}) \begin{Bmatrix} \phi(\mathcal{Q}) \\ \phi_t(\mathcal{Q}) \end{Bmatrix} = \int_S \begin{Bmatrix} \phi(\mathcal{P}) \\ \phi_t(\mathcal{P}) \end{Bmatrix} \frac{\partial}{\partial n} \ln r(\mathcal{P}, \mathcal{Q}) - \ln r(\mathcal{P}, \mathcal{Q}) \begin{Bmatrix} \frac{\partial \phi(\mathcal{P})}{\partial n} \\ \frac{\partial \phi_t(\mathcal{P})}{\partial n} \end{Bmatrix} dS, \quad (2)$$

where \mathcal{P}, \mathcal{Q} are points on the boundary, n is outward normal direction of the boundary, $r(\mathcal{P}, \mathcal{Q})$ is distance between \mathcal{P} and \mathcal{Q} , $c(\mathcal{Q})$ represents the angle subtended at \mathcal{Q} by boundaries.

On the free-surface, kinematic boundary condition and dynamic boundary condition for zero atmospheric pressure are applied as

$$\frac{D\phi}{Dt} = -z + \frac{1}{2}(\nabla\phi)^2 \quad (3)$$

$$\frac{D\mathbf{x}}{Dt} = \nabla\phi, \quad (4)$$

where $\mathbf{x} = (x, z)$. On the body surface, impermeability condition with respect to ϕ is expressed as

$$\frac{\partial\phi}{\partial n} = V_n, \quad (5)$$

where V_n denotes the normal velocity of the body surface. Denoting translating and angular velocities of the body as \mathbf{v}_o and $\boldsymbol{\omega}$ respectively, V_n is written as

$$V_n = \mathbf{n} \cdot (\mathbf{v}_o + \boldsymbol{\omega} \times \mathbf{r}). \quad (6)$$

Impermeability condition on the body with respect to ϕ_t ¹⁴⁾ can be written as

$$\begin{aligned} \frac{\partial\phi_t}{\partial n} = & -k_n (\nabla\phi - \mathbf{v}_o - \boldsymbol{\omega} \times \mathbf{r})^2 + \mathbf{n} \cdot (\dot{\mathbf{v}}_o + \dot{\boldsymbol{\omega}} \times \mathbf{r}) \\ & + \mathbf{n} \cdot \boldsymbol{\omega} \times (\boldsymbol{\omega} \times \mathbf{r}) + \mathbf{n} \cdot 2\boldsymbol{\omega} \times (\nabla\phi - \mathbf{v}_o - \boldsymbol{\omega} \times \mathbf{r}) \\ & - \frac{\partial}{\partial n} \left(\frac{1}{2}(\nabla\phi)^2 \right), \end{aligned} \quad (7)$$

where k_n is curvature of body, $\dot{\mathbf{v}}_o, \dot{\boldsymbol{\omega}}$ are translating and angular accelerations of the body respectively.

On the floating body surface, $\dot{\mathbf{v}}_o, \dot{\boldsymbol{\omega}}$ can not be specified explicitly and implicit boundary condition should be applied. Denoting the inertia tensor of the floating body as \mathcal{M} and generalized normal vector of body surface as $\mathbf{N} = (\mathbf{n}, \mathbf{n} \times \mathbf{r})$, the implicit boundary condition is written as

$$\begin{aligned} \frac{\partial\phi_t}{\partial n} = & \mathbf{N} \mathcal{M}^{-1} \left\{ \int_{S_s} -\phi_t \mathbf{N} ds \right\} \\ & + \mathbf{N} \mathcal{M}^{-1} \left\{ \int_{S_s} \left(-z - \frac{1}{2}(\nabla\phi)^2 \right) \mathbf{N} ds + \mathbf{F}_g \right\} \\ & + q - \frac{\partial}{\partial n} \left(\frac{1}{2}(\nabla\phi)^2 \right), \end{aligned} \quad (8)$$

where \mathbf{F}_g is sum of gravity, mooring force and other external forces acts to the body and q is the term which can be explicitly evaluated from the solution of velocity field as

$$q = -k_n (\nabla\phi - \mathbf{v}_o - \boldsymbol{\omega} \times \mathbf{r})^2 + \mathbf{n} \cdot \boldsymbol{\omega} \times (\boldsymbol{\omega} \times \mathbf{r}) + \mathbf{n} \cdot 2\boldsymbol{\omega} \times (\nabla\phi - \mathbf{v}_o - \boldsymbol{\omega} \times \mathbf{r}). \quad (9)$$

With these boundary conditions and Green's second identity with respect to ϕ and ϕ_t , both velocity and acceleration fields can be solved numerically by BEM. The solutions are integrated with respect to time by 4th order Runge-Kutta method, then fluid and the body motions are simulated in time domain. The free-surface is traced by MEL ⁴⁾.

Artificial damping zone

Following a preceding work of Cointe et al. ⁷⁾, damping terms are added to dynamic and kinematic free-surface boundary conditions to give artificial damping effect to free-surface. The free-surface boundary conditions inside a damping zone are given as

$$\frac{D\phi}{Dt} = -z + \frac{1}{2}(\nabla\phi)^2 - \nu(x_e)(\phi - \phi_e) \quad (10)$$

$$\frac{D\mathbf{x}}{dt} = \nabla\phi - \nu(x_e)(\mathbf{x} - \mathbf{x}_e). \quad (11)$$

where $\nu(x_e)$ is the damping coefficient

$$\nu(x) = \begin{cases} \alpha\omega\left(\frac{x-x_0}{\lambda}\right)^2, & \text{for } x_0 \leq x \leq x_1 = x_0 + \beta\lambda \\ 0, & \text{for } x < x_0 \text{ or } x > x_1 \end{cases}. \quad (12)$$

In the definition of $\nu(x)$, ω and λ are angular frequency and wave length of the incident wave respectively. The performance of this damping zone is controlled by two nondimensional parameter α and β . α is used to control the strength of damping and β is used to control the length of damping zone. ϕ_e, \mathbf{x}_e are reference values. This damping zone damps down differences $\phi - \phi_e$ and $\mathbf{x} - \mathbf{x}_e$. When the damping zone is applied in front of a rigid wall and works as a simple absorber, the reference values are set to $\phi_e = 0, \mathbf{x}_e = (x_e, 0)$. And when the damping zone is applied in front of a wave maker and works as an absorbing wave maker, the reference values are set to the solution of the wave generated by the wave maker. This solution can be computed by numerical simulation of the wave without bodies in the tank. For practical purpose, linear analytical solution can be a good substitution.

Linear propagating wave generated by a piston wave maker is described as

$$\phi(x, z, t) = \frac{4s \tanh kh \sinh kh}{\omega(2kh + \sinh 2kh)} \cosh k(z + h) \cos(kx - \omega t) \quad (13)$$

$$\eta(x, t) = -\frac{\partial \phi}{\partial t} \Big|_{z=0} = \frac{4s \sinh^2 kh}{2kh + \sinh 2kh} \sin(kx - \omega t) \quad (14)$$

where s is stroke of the wave maker and k is wave number of the generated wave. Wave reflection coefficient of this damping zone is less than 2%, when the tuning parameter is appropriately set to $\alpha = \beta = 1$ for a regular wave. ^{7, 15).}

SIMULATION WITH EXPERIMENTAL VALIDATION

Experiment

The experiment was performed in the sea-keeping test basin of Ship Research Institute. Fig.2 shows the plan and side views of the test basin and Fig.3 shows the section shape of the test model used in the experiment. To keep two-dimensionality, the test model was set between the rigid current plates installed in the center of the test basin. Fig.4 shows the measuring equipment of the motions. The swaying carriage is moored by weak and linear springs in horizontal direction to restrict free drifting. The principal dimensions of the model and measuring equipment are give in Table 1 and Table 2.

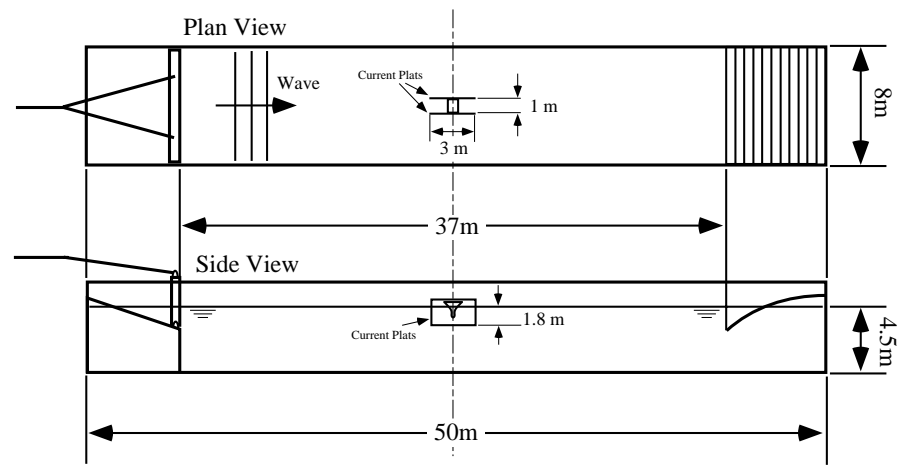


Fig.2 Test basin used for the experiment

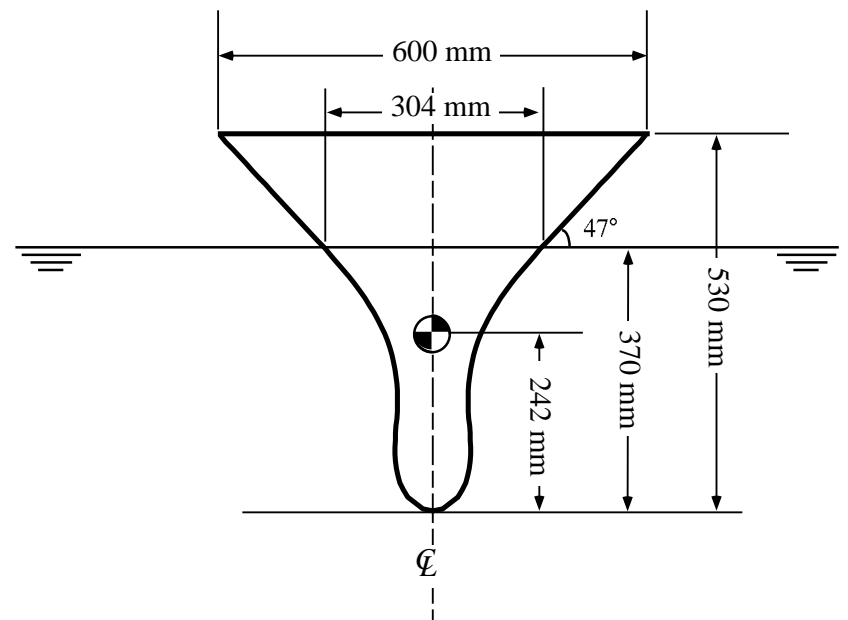


Fig.3 Body shape of the bow section model

Table 1 Principal dimensions of the bow section body

Item		M-K-S system
Breadth	B	0.600 m
Breadth at W.L.	$B_{W.L.}$	0.304 m
Depth	D	0.532 m
Length	L	0.997 m
Draft	d	0.370 m
Displacement	W	48.55 kg
Center of inertia	KG	0.242 m
Radius of inertia	R_I	0.193 m
Metacenter height	GM	0.032 m
Natural period of heave	T_h	1.07 sec
Natural period of roll	T_r	2.66 sec

Table 2 Principal dimensions of the measuring equipment

Swaying carriage	Weight	5875 g
	Measuring span	± 40 cm
Heaving rod	Weight	453 g
	Measuring span	± 20 cm
Gimbal	Weight	525 g
	Measuring angle	$\pm 30^\circ$
Load cell	Weight	137 g
	Capacity	± 5 kgf
Mooring system	Balance weight	500 g
	Spring constant	51.07 N/m

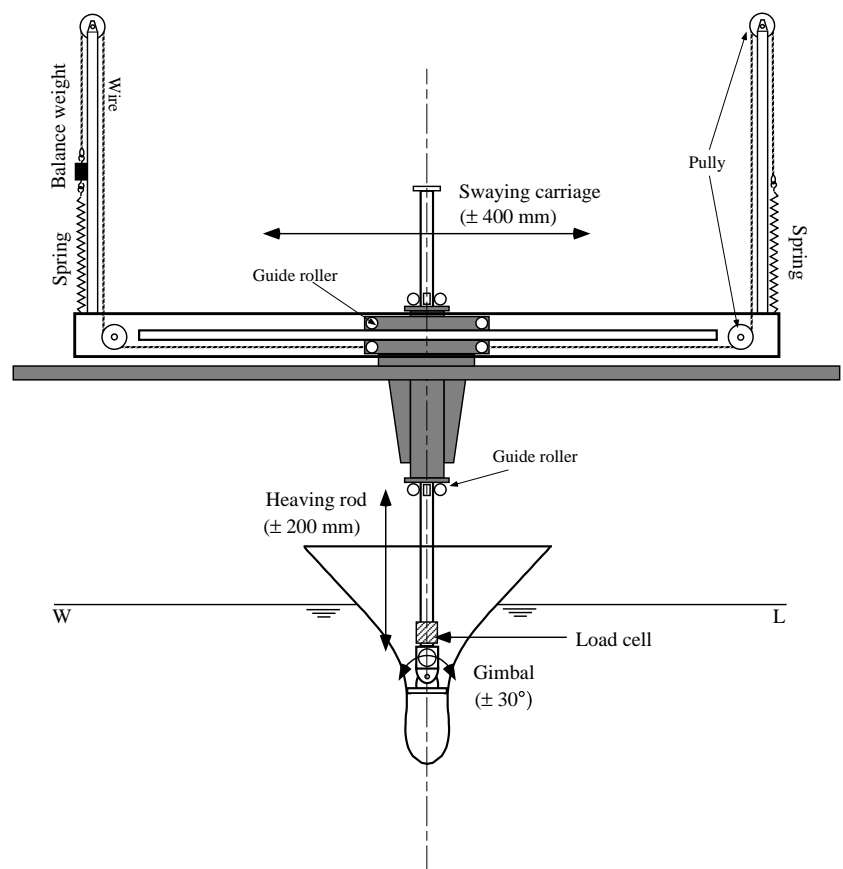


Fig.4 Measuring equipment

Comparison between simulated and measured body motions

First, harmonic body motions in a regular wave are compared. In Fig.5, simulated motions are plotted with measured motions. The length and height of the incident wave are $\lambda = 1.4m$ and $h_w = 5cm$ respectively. In this wave, the harmonic motions are dominant in both simulation and experiment. As the figure shows, the body motions are converging to the periodically steady harmonic motions after the transient motions. The low-frequency horizontal motion due to mooring is also damping down gradually around the position where the restoring force of the mooring balances with the steady wave drift force. The simulated harmonic motions of the body agree with the measured motion in overall.

Next, body motions in a different wave are compared in Fig.6. The length and height of the incident wave are $\lambda = 3.6m$ and $h_w = 8cm$ respectively. In this wave, roll motions are not harmonic and significant double period oscillations are observed both in simulation and experiment. This double period oscillation is the typical characteristic of the

parametric oscillation. When damping is linear, the parametric motion does not have a limit cycle and diverges exponentially. As this figure shows, the simulated motions well describe the exponential growth of the parametric oscillation and agreement with the measured motions are very good. The growth speed of roll angle in the simulation is faster than that of measured motion because the viscous effect is not considered in the simulation.

To visualize this parametric roll motion, simulated instantaneous positions of the body at $t/T_w = 21.25, 21.50, \dots, 25.00$ are plotted in Fig.7, where T_w is the period of the incident wave. Horizontal thin lines are calm water surface. The positions arranged in the same row are distant $2T_w$ in time. We can observe that the parametric roll motion is excited by the heave motion like a swing pumping and its growth is very natural. The amplitude of roll motion is large but wave radiation is not significant and no wave breaking is occurred near the body. The same natural and smooth parametric roll motions are observed also in the experiment.

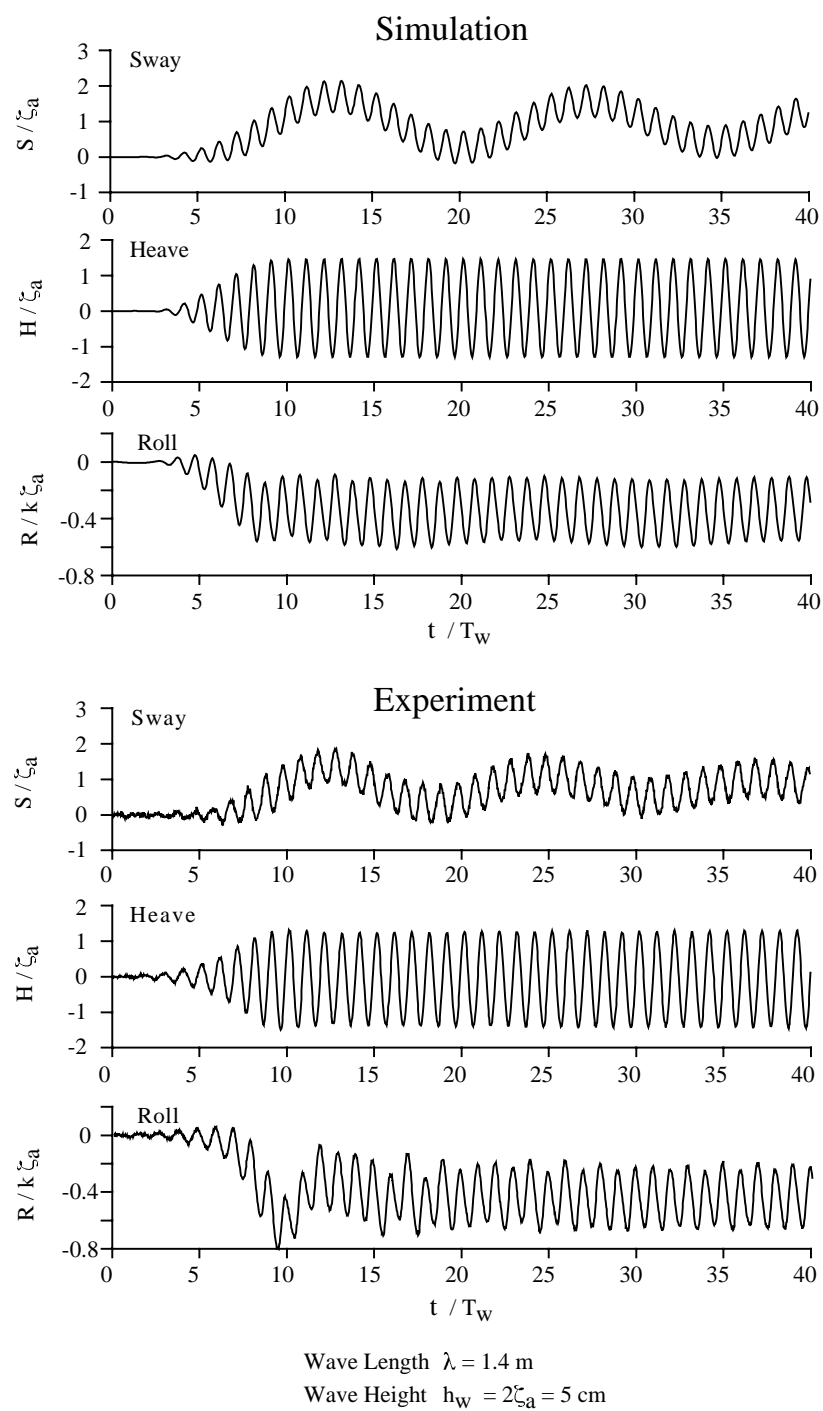


Fig. 5 Comparison of body motions between simulation and experiment

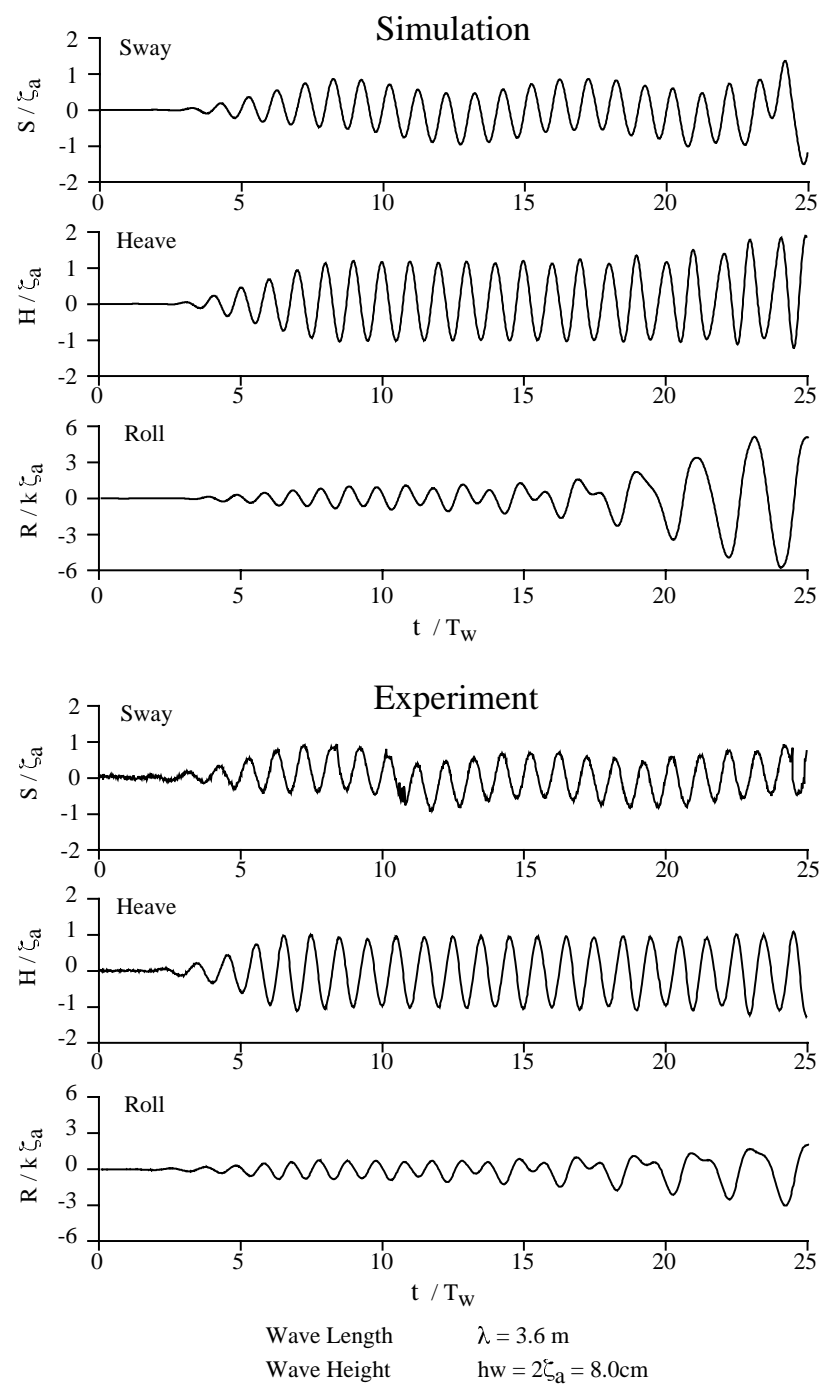


Fig.6 Comparison of body motions between simulation and experiment

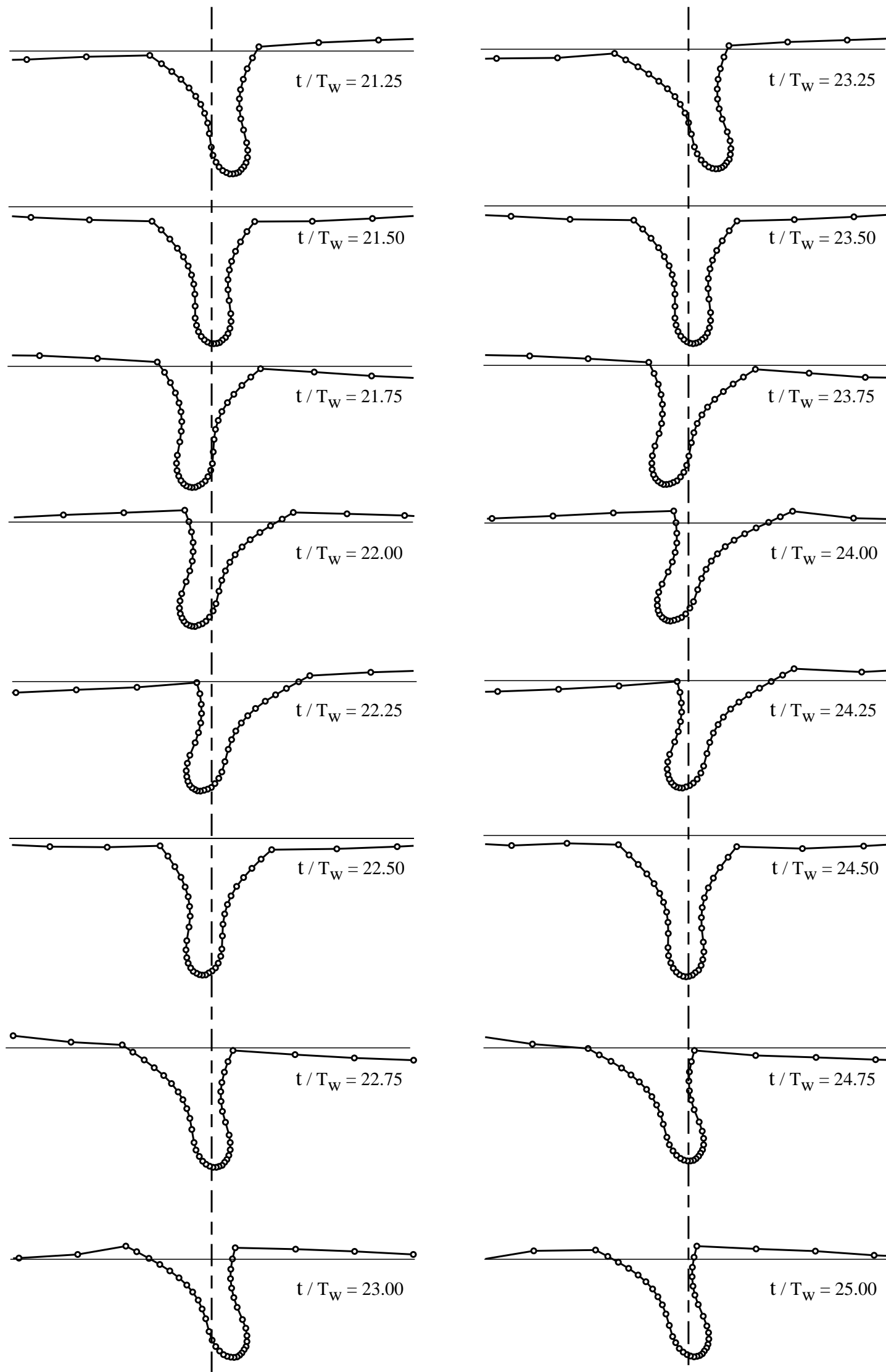


Fig.7 Simulated parametric motions of the bow section body

To observe the velocity and hydrodynamic pressure field, contour plots of the velocity potential ϕ and its time derivative ϕ_t at $t/T_w = 24.00$ are presented in Fig.8 and Fig.9. Since the boundary value problem on ϕ_t is solved in the simulation, the computation of ϕ_t distribution in the fluid domain is also simple and accurate.

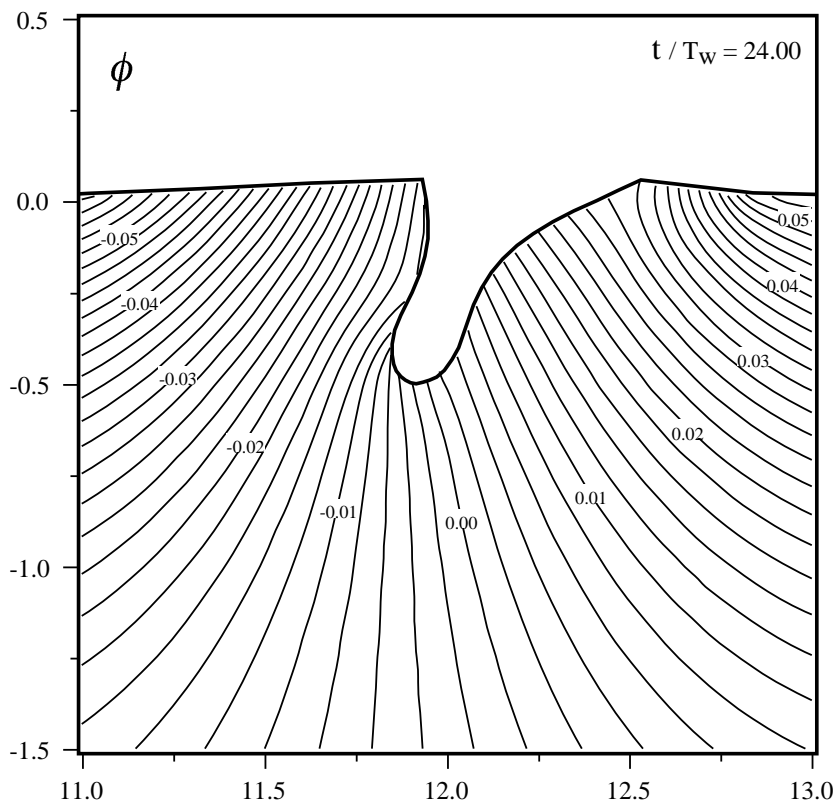


Fig.8 Contour plot of ϕ

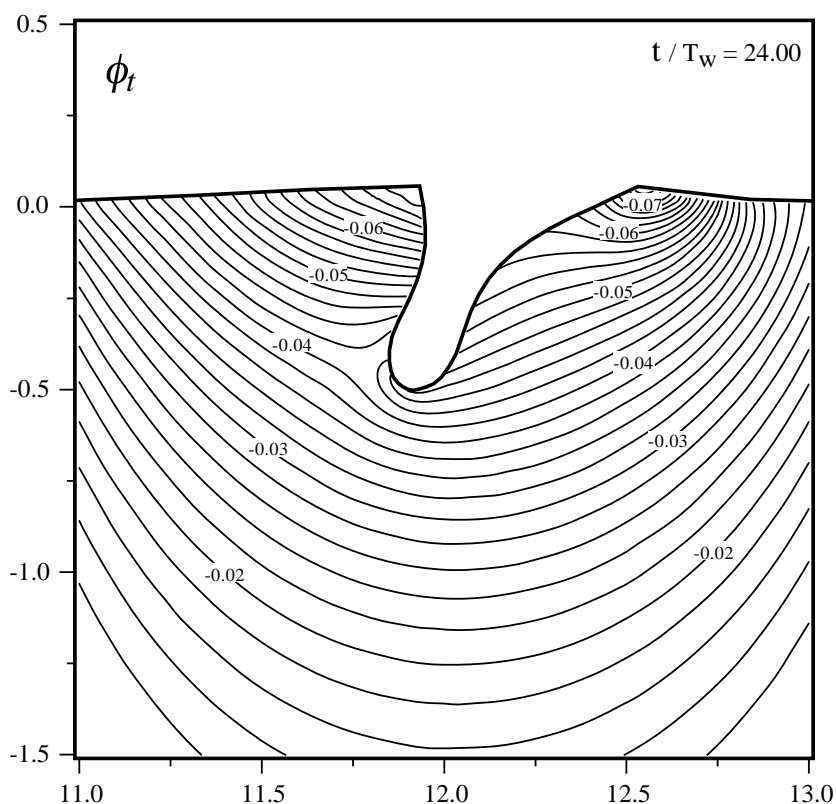


Fig.9 Contour plot of $\partial\phi/\partial t$

Analysis of the critical wave height of the parametric motions

First, the critical wave height determined by the experiment is shown in Fig.10. Combinations of the length and height of the incident wave used in the experiment are plotted. The \triangle marks indicate that the body motions are harmonic in that wave and the ∇ marks indicate

that they are parametric. When the body motions are parametrically excited, the significant double period oscillations are observed. As this figure shows, motions are harmonic when wave height is low. And when wave height is higher than the critical level, the parametric oscillation is excited. The thick solid line drawn between \triangle and ∇ is the critical wave height determined experimentally.

Next, numerical results are plotted in Fig.11. The \triangle marks indicate that the simulated body motions are harmonic and the ∇ marks indicate that they are parametric. The thick broken line drawn between \triangle and ∇ is the critical wave height determined numerically.

For the theoretical study of the critical wave height, Mathieu type model equation is usually used. The critical wave height is given as the eigenvalues of the Mathieu equation. The Mathieu type simultaneous model equations of heave and roll motions can be written as

$$\ddot{z}_G + c_1 \dot{z}_G + a_1(z_G - \xi) = 0 \quad (15)$$

$$\ddot{\theta} + c_2 \dot{\theta} + a_2(\theta - \xi_x) + b_2(z_G - \xi)(\theta - \xi_x) = 0, \quad (16)$$

where z_G, θ, ξ, ξ_x are nondimensional heave, roll, free-surface elevation and free surface slope respectively and $a_1 \sim c_2$ are coefficients determined from the hydrodynamic and hydrostatic property of the body. The values of the coefficients are

a_1	2.839	—	—	c_1	0.7308
a_2	0.3495	b_2	9.783	c_2	0.02541

To determine the eigenvalues of eq.(16), exciting force is not important and can be neglected. The damping term can be removed by substituting $\vartheta e^{-c_2(z_G - \xi)/2}$ for θ . But, since damping coefficient c_2 is so small that we can simply neglect the damping term to have

$$\ddot{\vartheta} + \{a_2 + b_2(z_G - \xi)\}\vartheta = 0. \quad (17)$$

The relative heave motion of body to free-surface $z_G - \xi$ can be approximated as

$$z_G - \xi = \xi_r \cos \omega t, \quad (18)$$

then equation of roll motion is reduced to be a Mathieu equation

$$\ddot{\vartheta} + \{a_2 + b_2 \xi_r \cos \omega t\}\vartheta = 0. \quad (19)$$

The relation between ξ_r and the amplitude of the incident wave ξ_a can be given from eq.(15) as

$$\xi_r = \frac{\sqrt{\omega^4(a_1 - \omega^2 + c_1^2)^2 + a_1^2 c_1^2 \omega^2}}{(a_1 - \omega^2)^2 + c_1^2 \omega^2} \xi_a. \quad (20)$$

The critical wave height given from eq.(19) is plotted together with the experimental and the numerical values in Fig.12. The region above the wave slope 1/10 has no practical meaning. This theoretical result qualitatively agrees with the experimental result, meanwhile the numerical result agrees with the experimental result qualitatively and quantitatively. In the numerical simulation, the parametric motions are excited in little lower waves than those of in experiment. This difference is considered to result from the viscous effect.

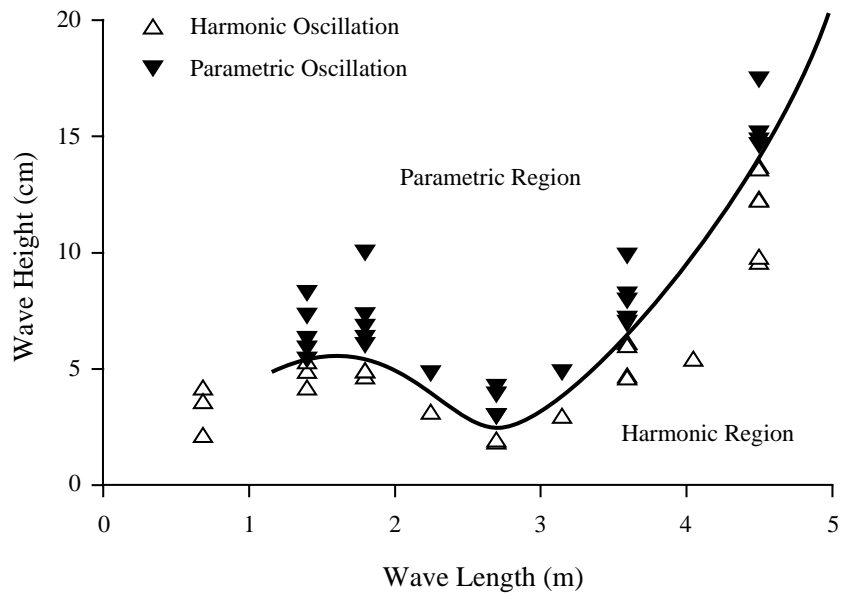


Fig.10 Criteria of parametric and harmonic regions given by experimentation

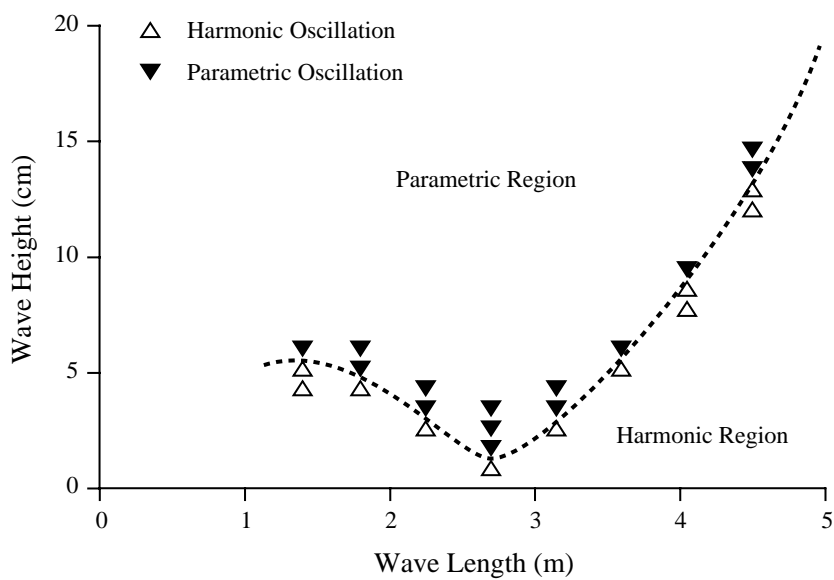


Fig.11 Criteria of parametric and harmonic regions given by the nonlinear simulation

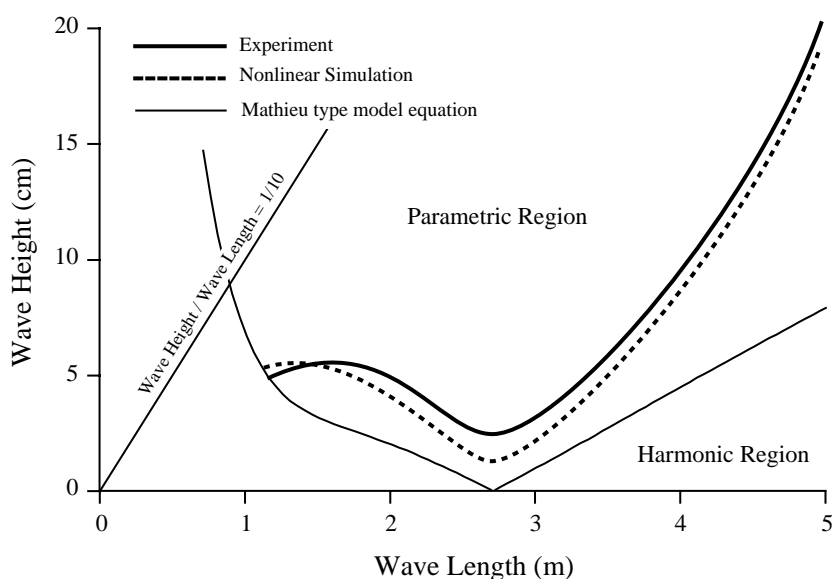


Fig.12 Criteria of parametric and harmonic regions. Comparison among experiment, the nonlinear simulation and the Mathieu type model equations

CONCLUSION

In this study, the fully nonlinear numerical wave tank is applied to simulate parametric roll motions of a two-dimensional floating body and the critical wave height is determined. The results are validated

by the experiment. The following items are main conclusions.

1. The simulated harmonic body motions well agree with the measured harmonic motions in overall.
2. The simulated parametric motions also agree with the measured parametric motions.
3. The critical wave height analyzed by Mathieu type model equation agree with the experimental results qualitatively.
4. The critical wave height determined by the simulation well agree with the experimental results quantitatively.

In conventional analysis of the harmonic, parametric and the other nonlinear motions of floating bodies, the interaction between wave and floating bodies is represented as hydrodynamic coefficients. These coefficients are given from linear or perturbation theories in general. But now, we have fully nonlinear numerical wave tank. With this new technology, the nonlinear interaction can be directly simulated in time domain. The parametric roll motion is only one application of the numerical wave tank. This powerful and rational tool can be applied to a variety of nonlinear problems.

REFERENCES

- 1) Hsu, C.S. (1977), "On nonlinear parametric excitation problems", *Advances in Applied Mechanics*, Vol.17, pp245-298
- 2) Skomedal, N.G. (1982), "Parametric excitation of roll motion and its influence on stability", *Proc. of 2nd Int. Conf. on Stability of Ships and Ocean Vehicles, Tokyo*, pp113-125
- 3) Kyojuka, Y. (1977), "A study on the unstable roll motions of moored floating bodies in regular waves.", *Master thesis, Osaka Univ.*, pp1-82
- 4) Longuet-Higgins, M.S. and Cokelet, E. (1976), "The deformation of steep surface waves on water", *Proc. Roy. Soc. ser.A350*, pp1-26
- 5) Vinje, T. and Brevig, P. (1981), "Nonlinear Ship Motions", *Proc. of the 3rd. Int. Conf. on Num. Ship Hydro.*, ppIV3-1-IV3-10
- 6) Sen, D., Pawlowski, J.S., Lever, J. and Hinchey, M.J., (1989), "Two-dimensional numerical modeling of large motions of floating bodies in waves", *Proc. 5th Int. Conf. Num. Ship Hydro., part1*, pp257-277
- 7) Cointe, R., Geyer, P., King, B., Molin, B. and Tramon, M. (1990), "Nonlinear and linear motions of a rectangular barge in perfect fluid", *Proc. of the 18th Symp. on Naval Hydro., Ann Arbor, Michigan*, pp85-98
- 8) Tanizawa, K. (1990), "A numerical method for nonlinear simulation of 2-D body motions in waves by means of B.E.M.", *Journal of SNAJ*, Vol.168, pp223-228
- 9) Kang, C.G., and Gong, I.Y. (1990), "A numerical solution method for three-dimensional nonlinear free-surface problems", *Proc. of the 18th Symp. on Naval Hydro., Ann Arbor, Michigan.*, pp427-438
- 10) Van Daalen, E.F.G. (1993), "Numerical and Theoretical Studies of Water Waves and Floating Bodies", *Ph.D. thesis, University of Twente, The Netherlands*
- 11) Sen, D. (1993), "Numerical simulation of motions of two-dimensional floating bodies", *Journal of Ship Research*, vol.37, pp307-330
- 12) Cao, Y., Beck, R. and Schultz, W.W. (1994), "Nonlinear motions of floating bodies in incident waves", *9th Workshop on Water Waves and Floating Bodies, Kuju, Oita*, pp33-37
- 13) Tanizawa, K. (1995a) "A Nonlinear Simulation Method of 3-D body Motions in Waves", *10th Workshop on Water Waves and Floating Bodies, Oxford*, pp235-239
- 14) Tanizawa, K. (1995b) "A Nonlinear Simulation Method of 3-D Body Motions in Waves", *Journal of SNAJ*, Vol.178, pp179-191
- 15) Tanizawa, K. (1996) "Long time fully nonlinear simulation of floating body motions with artificial damping zone", *Journal of SNAJ*, Vol.180, pp311-319